Radiometric Modeling of Mechanical Draft Cooling Towers to Assist in the Extraction of their Absolute Temperature from Remote Thermal Imagery

Matthew Montanaro[a], Carl Salvaggio[a], Scott D. Brown[a], David W. Messinger[a], Alfred J. Garrett[b], and James S. Bollinger[b]

[a]Rochester Institute of Technology, 54 Lomb Memorial Drive, Rochester, NY, USA;
[b]Savannah River National Laboratory, Building 735-A, Office B108, Aiken, SC, USA

ABSTRACT

Determining the internal temperature of a mechanical draft cooling tower (MDCT) from remotely-sensed thermal imagery is important for many applications that provide input to energy-related process models. The problem of determining the temperature of a MDCT is unique due to the geometry of the tower and due to the exhausted water vapor plume. The radiance leaving the tower is dependent on the optical and thermal properties of the tower materials (*i.e.*, emissivity, BRDF, temperature, etc.) and also the internal geometry of the tower. The tower radiance is then propagated through the exhaust plume and through the atmosphere to arrive at the sensor. The expelled effluent from the tower consists of a warm plume with a higher water vapor concentration than the ambient atmosphere. Given that a thermal image has been atmospherically compensated, the remaining sources of error in extracted tower temperature due to the exhausted plume and the tower geometry must be accounted for. A temperature correction factor due to these error sources will be derived through the use of three-dimensional radiometric modeling. A range of values for each important parameter are modeled to create a target space (*i.e.*, look-up table) that predicts the internal MDCT temperature for every combination of parameter values. This LUT, along with user knowledge of the scene, provides a means to convert the image-derived apparent temperature into the estimated absolute temperature of a MDCT. Preliminary results indicate that temperature error corrections of approximately 1 - 9 Kelvin can be achieved with the range of MDCT parameters encompassed by the LUT.

Keywords: PHYSICS MODELING, TARGET SPACE, SYNTHETIC IMAGE GENERATION, APPARENT TEMPERATURE, THERMAL INFRARED

1. INTRODUCTION

Knowledge of the absolute temperature of a surface is useful for a wide range of applications ranging from environmental to industrial to security. The objective is to estimate the temperature of the air exiting a mechanical draft cooling tower (MDCT) through the use of remote thermal imagery. Knowledge of the temperature of the cooling towers is necessary for input into process models that yield information about the industrial processes that the cooling towers service. Visible and thermal images of such cooling towers are displayed in Figure 1.

A camera sensitive to the LWIR spectral region (approximately 8 - 14 μm) is used to observe the cooling tower. Each pixel in the resulting thermal image is converted into an apparent temperature, or image-derived temperature. The apparent temperature of pixels inside the fan stack opening of the tower is to be correlated to the exit air temperature. To do so, full 3-D modeling of the radiation transfer is necessary to accurately derive the exhaust air temperature from the thermal image. A sensor model is necessary to derive the apparent temperature of the MDCT from the simulated image for a particular sensor. Finally, a target space is constructed to predict the apparent temperature of the MDCT for a range of model parameters. This target space information will allow a temperature correction factor to be assembled that will be applied to the thermal image to produce an accurate MDCT temperature.

Send correspondence to Matthew Montanaro: E-mail: mxm9876@cis.rit.edu

(a) Visible color image (b) LWIR image

Figure 1. Mechanical draft cooling towers at the Savannah River National Laboratory.

A MDCT operates on the concept of evaporative cooling. Heated water from an industrial process is pumped through the tower. The water is exposed to cooling air streams which will tranfer heat from the water to the air. The temperature of this warm air is of interest. A methodology is developed to derive the temperature of the exhausted air from a remotely sensed thermal image.

2. BACKGROUND

Radiance from the cooling tower may be significantly altered before it is recorded by the sensor.

2.1 Tower-Leaving Radiance

Radiance leaving the tower consists of a self-emitted term and a reflected background term written as

$$L_{tower}(\theta,\phi,\lambda) = \varepsilon(\theta,\phi,\lambda)L_{BB}(\lambda,T) + \int_{2\pi} L_{bkgd}(\theta_i,\phi_i,\lambda)\,\rho'(\theta_i,\phi_i,\theta,\phi,\lambda)\cos(\theta_i)d\omega_i, \qquad \left[\frac{W}{m^2\,sr\,\mu m}\right] \tag{1}$$

where $L_{BB}(\lambda,T)$ is the Planck blackbody spectral radiance, $L_{bkgd}(\theta_i,\phi_i,\lambda)$ is the radiance downwelled onto the tower from the (θ_i,ϕ_i) direction, and (θ,ϕ) indicate the direction of the sensor. The function $\varepsilon(\theta,\phi,\lambda)$ is the directional hemispherical emissivity (DHE). Its value is between zero and unity and indicates the effectiveness of an object as a radiator.

The function $\rho'(\theta_i,\phi_i,\theta,\phi,\lambda)$ is known as the bidirectional reflectance distribution function (BRDF). It is defined as the ratio of the radiance, L, reflected from the surface into the direction (θ_r,ϕ_r) to the irradiance, E, incident on the surface from direction (θ_i,ϕ_i) [1]. The BRDF describes the distribution of reflected radiance into the hemisphere from a given source geometry.

The integral of the BRDF over the hemisphere yields the directional hemispherical reflectance (DHR),

$$\rho(\theta_i,\phi_i,\lambda) = \int_{2\pi} \rho(\theta_i,\phi_i,\theta_r,\phi_r,\lambda)\cos(\theta_r)d\omega_r. \tag{2}$$

Through Kirchhoff's assumptions, the DHE and DHR for an opaque object of interest are related by

$$\epsilon(\theta,\phi,\lambda) + \rho(\theta,\phi,\lambda) = 1. \tag{3}$$

From equation (1), it is apparent that the tower-leaving radiance will be affected by the background radiance and on the optical properties of the tower. The background radiance will depend on the geometry of the tower and on the downwelling radiance incident upon the tower. The optical properties consist of the BRDF and directional emissivity of the tower materials.

2.2 Sensor-Reaching Radiance

Radiance leaving the tower cavity must now propagate through the intervening column of air between the tower and the sensor. The atmosphere will both attenuate and exaggerate the signal through transmission losses, $\tau(\lambda)$, and additive upwelling radiance, $L_u(\lambda)$. The radiance reaching the front of the sensor after passing through the air column is

$$L(\theta, \phi, \lambda) = \tau(\theta, \phi, \lambda)\, L_{tower}(\theta, \phi, \lambda) + L_u(\theta, \phi, \lambda) \qquad \left[\frac{W}{m^2\, sr\, \mu m}\right]. \tag{4}$$

2.3 Sensor

The radiance is then incident on the sensor. The sensor first collects the incident radiation and focuses it on the focal plane. The collection process may distort the image due to diffraction and other effects. The point-spread function (PSF) is a measure of the blur introduced by the imaging system. For a typical optical system with a circular aperture, the PSF is an Airy disc function [2]. The Airy disc consists of concentric rings of decreasing intensity. The spread of the Airy pattern is usually reported by r_0 which is the distance on the focal plane from the center of the disc to the first minimum ring. Mathematically, the blurred image on the focal plane is the two-dimensional convolution of the PSF with the incoming radiance field.

Detectors located at the focal plane respond to the radiance incident on them. Since the detectors have a finite spatial width, a loss of spatial detail occurs as a result of this process. The width of the detector elements, the focal length, and the distance from the sensor to the target all determine the ground sampling distance (GSD) of the sensor.

Finally, the sensor spectrally samples the incoming spectral radiance. The sensor is only responsive to a certain range of wavelengths. The responsivity of the sensor to each wavelength is represented by the spectral response function, $R'(\lambda)$. It is a unitless value between zero and unity describing the fraction of radiation that is recorded by the sensor at a particular wavelength. The spectral radiance is weighted by the response function by wavelength and then integrated to arrive at an integrated band radiance. This integrated radiance may then be converted into an apparent temperature. The end result is an image-derived apparent temperature that will most likely be different from the absolute temperature of the target. This temperature diffence must be accounted for.

3. PHYSICS MODEL

The Digital Imaging and Remote Sensing Image Generation (DIRSIG) software [3] developed at Rochester Institute of Technology (RIT) and the MODerate spectral resolution TRANsmittance (MODTRAN) software [4] developed by the Air Force Research Laboratory (AFRL) are used to model the internal and propagated radiometry of the MDCT. The parameters used in these simulations are listed here along with a detailed description of how they will be modeled. Eventually, every combination of parameter values will be used to create a target space (look-up table) that will predict the at-sensor radiance and therefore the necessary temperature correction factor.

3.1 Tower Leaving Radiance with DIRSIG

The tower-leaving radiance is modeled using DIRSIG. This radiance includes the self-emitted radiance and any reflected radiance from the tower facets. The simulation is based on a CAD drawing of a MDCT that is shown in Figure 2. A previous study confirmed that DIRSIG is able to produce a radiometrically accurate representation of a MDCT [5].

The facets of the CAD drawing are assigned a Ward BRDF model [6]. The mathematical formulation of the BRDF model is

$$\rho'\left(\theta_i, \phi_i, \theta_r, \phi_r\right) = \frac{\rho_d}{\pi} + \frac{\rho_s}{\sqrt{\cos\theta_i\, \cos\theta_r}} \frac{\exp\left[-\tan^2\alpha/\sigma^2\right]}{4\pi\sigma^2} \qquad \left[\frac{1}{sr}\right]. \tag{5}$$

The model's input parameters are the diffuse reflectance component, ρ_d, the specular reflectance component, ρ_s, and the surface roughness, σ. The σ parameter essentially controls the width of the specular lobe. The diffuse

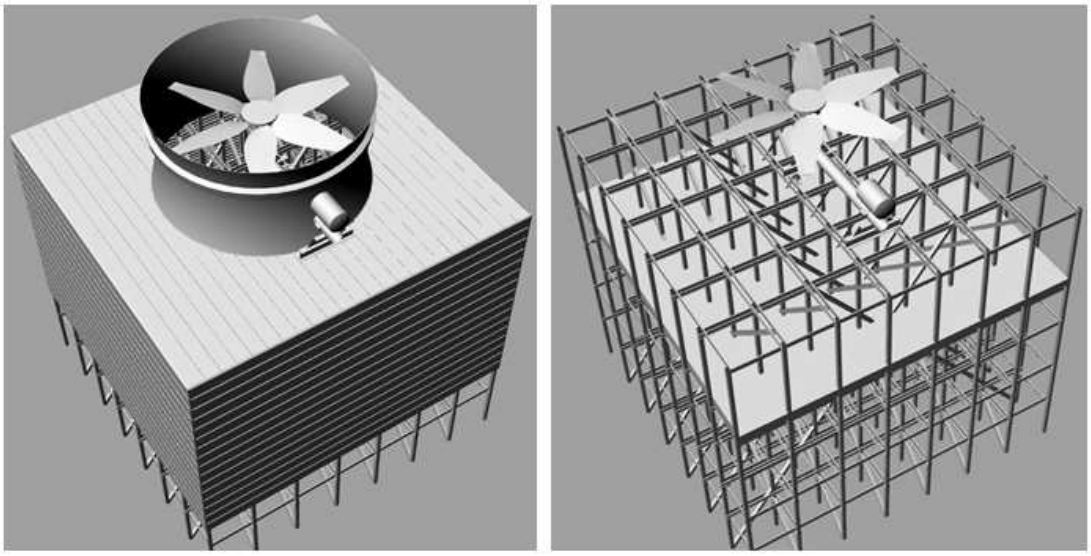

Figure 2. CAD drawing of a counter-flow MDCT exterior view (left) and interior view (right).

and specular weights of the Ward BRDF model are adjusted to provide a mostly specular reflectance with a small diffuse component. The Ward parameters for this BRDF model are $\rho_d = 0.12$, $\rho_s = 0.03$, and $\sigma = 0.10$. This BRDF shape is consistent with typical MDCT construction materials found in the Nonconvential Exploitation Factors Data System (NEFDS) [7]. Figure 3(c) illustrates the BRDF shape used for the DIRSIG model. The reflectance (DHR) of this BRDF when measured from an angle of 20° is 0.15. Therefore, the emissivity (DHE) is 0.85 through Kirchhoff's relation. The measurement angle of 20° was selected to keep the model consistent with emissivity measurements of MDCT construction materials. Every facet in the CAD model was assigned this BRDF.

The DIRSIG simulation provides a spatially and spectrally over-sampled tower-leaving radiance. The output image is 110 by 110 pixels that cover the entire fan stack opening and part of the tower deck. The ground sampling distance (GSD) of this over-sampled image is 0.05 meters. The image covers the longwave infrared (LWIR) wavelength regions at a spectral resolution of one wavenumber.

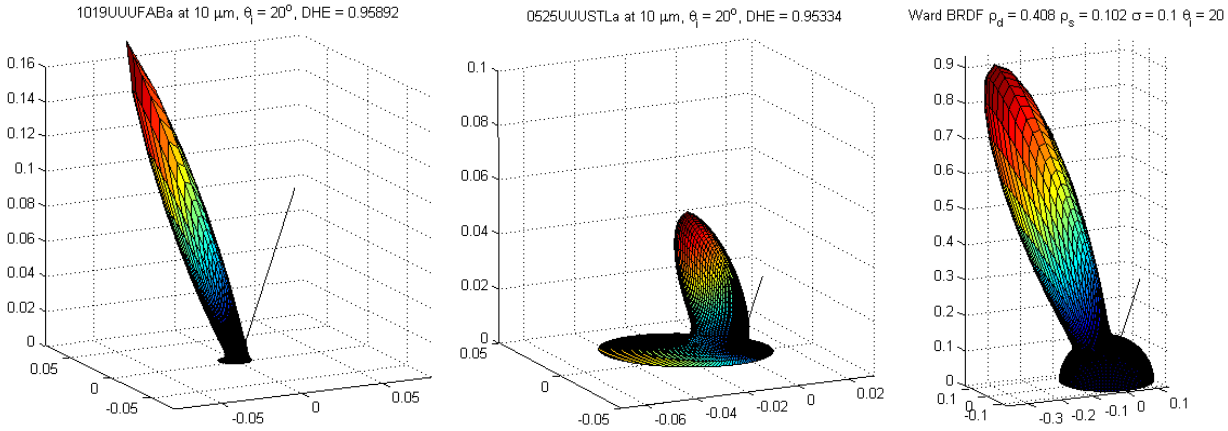

(a) Weathered Galvanized Steel (b) Weathered Plastic (c) Ward BRDF

Figure 3. NEFDS material LWIR BRDFs (a) and (b) and the Ward BRDF model assigned to the facets in the DIRSIG CAD model.

DIRSIG Parameters

The list of DIRSIG parameters that will be varied for the target space are presented here.

MDCT Internal Temperature is the temperature assigned to the internal facets of the MDCT DIRSIG model. These internal facets include the interior faces of the decking and siding, the drift eliminator baffles, the internal tower support structures, the fan support structure, and the fan mechanical structures. This internal temperature is important since it is the desired temperature to be retrieved from the remotely-sensed image.

MDCT External Temperature is the temperature assigned to the exterior facets of the MDCT DIRSIG model. These external facets include the exterior faces of the decking and siding, the shroud (cowling), and the fan blades. The important external facets for the physics model are the fan blades and the shroud since these objects are in the line-of-sight between the sensor and the tower cavity.

The external temperature is set to be less than or equal to the assigned internal temperature (assuming nighttime imaging only). From the MDCT collect performed at SRNL in the spring of 2004 and 2005, the external apparent temperatures appear to be between 0 and 4 Kelvin less than the internal temperature for the nighttime scenes.

Fan Blade Emissivity can be adjusted by altering the Ward BRDF model parameters for the fan blade facets. The Fan Blade Emissivity parameter is used to scale the magnitude of the BRDF assigned to the fan blades. To do so, a reference Ward BRDF is set in which the diffuse and specular weights were chosen to produce the desired BRDF shape of a mostly specular lobe with a small diffuse component ($\rho_d = 0.0408$ and $\rho_s = 0.0102$). The integral of this BRDF shape yields a DHR of 0.05 for a measurement angle of 20°. To scale the magnitude of this BRDF while maintaining its shape, the diffuse and specular weights are adjusted by

$$[\rho_d\,,\,\rho_s] = \frac{1-\varepsilon_{fan}}{0.05}\,[0.0408\,,\,0.0102]\,. \tag{6}$$

Effective Sky Temperature is the apparent temperature of the sky computed from the integrated downwelling sky radiance. This is the equivalent blackbody temperature of the sky. It can be computed from a known atmospheric temperature and moisture profile (sonding). The profile is used as input into MODTRAN and the path radiance from sample points covering the entire sky hemisphere is computed. The downwelling radiance from the computed samples is integrated over the entire sky hemisphere and converted into an apparent temperature. The Effective Sky Temperature is used by DIRSIG to compute the downwelling radiance from each portion of the sky. This downwelling radiance is necessary since it reflects off the tower facets and therefore becomes a component of the tower-leaving radiance.

Sensor Zenith Angle is the view angle of the sensor measured relative to a nadir (downlooking) viewing position of the MDCT. The radiance leaving the tower has an angular distribution. The view angle is important since it determines what features of the tower, such as the tower cavity and shroud side, are visible by the sensor and may therefore be included in the interior radiance field due to optical, mechanical, and atmospheric blurring.

3.2 Plume Leaving Radiance with MODTRAN

The tower-leaving radiance produced by DIRSIG must now propagate through the exhausted water vapor plume to reach the sensor. The MODTRAN software is used to model the plume. A previous study revealed that knowledge of the water vapor content in the plume is important for accurate temperature retrieval [8]. A standard atmosphere is first assigned to a user-defined atmosphere. A plume layer is then defined that extends from the ground to a height, z. The surface temperature in this profile is assigned the same value that was used for the *MDCT Internal Temperature* in the DIRSIG model since the assumption is made that the interior MDCT surfaces and the exit air are at the same temperature. Similarly, the surface dew point depression is set to zero since the assumption is made that the exit air is nearly saturated. The sensor is placed at the height of the plume

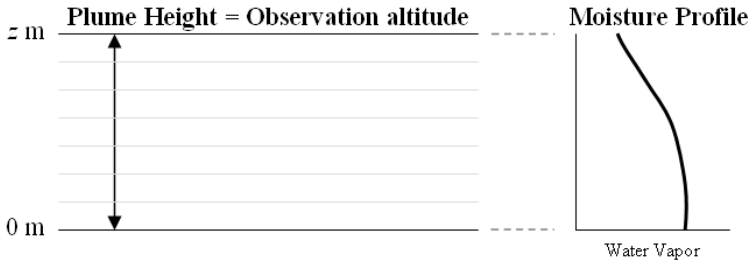

Figure 4. Illustration of atmospheric layers in MODTRAN used to model the moisture gradient in the plume.

layer (z) so that the atmospheric effect of the plume is isolated. Figure 4 illustrates this layout. A temperature and moisture gradient established in the atmospheric profile follows that of a Gaussian function. The temperature approaches the ambient air temperature as the height increases. Similarly, the dew point temperature approaches the ambient dew point temperature as the height increases. The height of the plume is defined as the two standard deviations distance of the Gaussian (2σ).

The MODTRAN simulation provides spectral atmospheric transmission and spectral atmospheric upwelling (path) radiance curves for the same spectral range as the DIRSIG simulation.

MODTRAN Parameters

The list of MODTRAN parameters that will be varied are presented here along with a description of each.

Ambient Air Temperature is the temperature of the ambient air measured at the surface. This value will be the final temperature the plume cools to.

Ambient Dew Point Temperature is the dew point temperature of the ambient air measured at the surface. This value will be the final dew point temperature of the plume.

Water Vapor Plume Path Length is the effective line-of-sight path length through the plume. This parameter is estimated by the user based on knowledge of the sensor view angle, air flow through the tower, and wind speed and direction. The plume path length is modeled as the height of the plume layer (z) in the MODTRAN user-defined atmosphere.

3.3 Physics Model Summary

Each spectral pixel in the DIRSIG tower-leaving radiance image is multiplied by wavelength with the spectral transmission data and then added by wavelength with the spectral path radiance from MODTRAN. The result of the DIRSIG and MODTRAN simulations is a sensor-reaching radiance that is spatially and spectrally over-sampled. Note that it is assumed that an atmospheric compensation has been performed on the image that removed the effect of the air column from the sensor to the top of the plume. Therefore, the result of the DIRSIG and MODTRAN run is essentially a "top of plume" radiance.

4. SENSOR MODEL

The high spatial and spectral resolution image generated by the physics model represents the radiance reaching the sensor. The sensor will degrade and record the radiance that enters the aperture. The sensor model accepts sensor specifications from the user and applies those specifications to the over-sampled physics model radiance image. An algorithm was written in the Matlab programming environment that processes the over-sampled image according to the sensor model provided by the user. Specifically, the spectral response, the GSD, and the radius of the system point spread function are necessary.

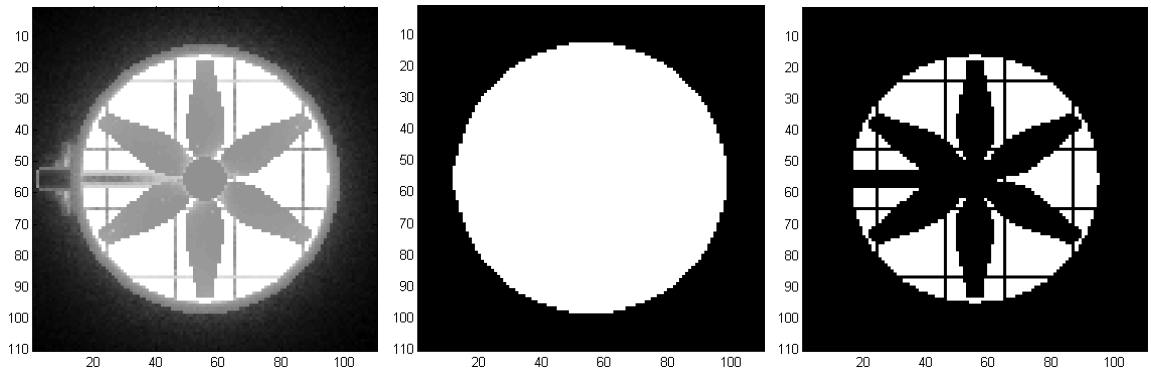

(a) (b) (c)

Figure 5. Over-sampled DIRSIG image (a) along with the mixed ROI (b) and cavity-only ROI (c) drawn for sensor angle of 0 degrees. White pixels in the masks indicate pixels that were included in the apparent temperature mean.

The sensor spectral response consists of a vector of wavelengths and a corresponding vector of response weights for a particular spectral band. The algorithm first spectrally samples the radiance images with the supplied spectral response. The spectral response function is resampled to the wavelengths used in the radiance image. The response function and the over-sampled image radiance are then multiplied together by wavelength for every pixel and integrated over all wavelengths to arrive at a band integrated image. This new image now consists of a single band but is still spatially over-sampled (110 by 110 pixels).

Next, a system point spread function (PSF) (modeled as an Airy disc) whose radius was provided by the user is applied to the image thereby blurring it. The user-supplied radius is in units of microns. The result of the PSF application is a blurred image that still consists of 110 by 110 pixels.

Finally, the image must be down-sampled such that the final image has the user required GSD. The GSD of the over-sampled radiance image is 0.05 meters. The user-supplied GSD is rounded to the nearest 0.05 meters so that the final GSD is an integer multiple of the original GSD to make the computations easier. The image is then divided into blocks whose dimensions are equal to the ratio of the new GSD to the original GSD. The mean value in each block is taken as the value of the corresponding pixel location in the final down-sampled image. For example, if the user required a GSD of 0.1 meters, the new-to-original GSD ratio would be two. Therefore, the image would be divided into 2 by 2 blocks and the mean radiance value in each 2 by 2 block is calculated. The final down-sampled image would be 55 by 55 pixels.

The result of the sensor application is a final down-sampled and band integrated image whose pixel GSD, system blur, and spectral band was specified by the user.

4.1 Region of Interest - Mixed vs. Cavity

The MDCT apparent temperature may now be derived from the processed images. Two region of interest (ROI) masks were created. The first mask covered the entire tower opening. The second mask was carefully constructed to avoid the fan blades and visible support structures so that only the cavity pixels were taken. Figure 5 illustrates the over-sampled images for a sensor zenith angle of 0° and the mixed and cavity ROIs for the radiance images. The same sensor model used on the over-sampled image is also applied to the ROI masks so that the masks fit the processed image.

The mean radiance for the pixels in each ROI is then calculated. The corresponding apparent temperature was found for each ROI. The temperature error was defined as the difference between the predicted apparent temperature (*i.e.*, ROI mean apparent temperature) and the assigned *MDCT Internal Temperature*. The temperature errors were calculated for both the mixed ROI and the cavity only ROI.

5. TARGET SPACE LOOK UP TABLE

The physics model and the sensor model generate a single simulated thermal image for a given set of parameter values and for a given sensor. This results in a predicted temperature error (temperature correction) for the set of parameter values. To be useful for an image analyst, a temperature correction must be known for any scene. Since the values of each of the eight parameters will probably not be known exactly, the physics model may be run many times with various parameter values. The resulting list of temperature correction factors for each combination of parameter values is known as a target space. This concept is similar to the target space used by Healey and Slater [9] and Ientilucci and Schott [10] for target detection . The target space is essentially a look-up table (LUT) that lists the predicted image-derived apparent temperature for a specific sensor for each combination of parameter values.

5.1 Parameterized Model

Multiple regression analysis may be performed on the LUT of temperature corrections. A multiple linear regression equation may be fit to the dataset to arrive at a single multi-parameter equation that predicts the temperature error given a set of parameter values. A multiple linear regression model has the form [11],

$$y_i = \beta_0 + \beta_{i,1}\, x_{i,1} + \beta_{i,2}\, x_{i,2} + ... + \beta_{i,p-1}\, x_{i,p-1} + \varepsilon_i \tag{7}$$

where the β variables are the model fit coefficients. A relationship between the response variable (the temperature error) and the predictor variables (the target-space parameters) is desired. Since the first target-space parameter, *MDCT Internal Temperature*, is the ultimate variable that is to be determined, it is not included in the regression model. The model predictors are therefore the other seven parameters.

The least-squares regression equation may be expressed in matrix form as

$$Y = X\,\beta + \varepsilon. \tag{8}$$

The predicted fit coefficients, b, are found by

$$b = (X'\,X)^{-1}\; X'\,Y. \tag{9}$$

Therefore, the predicted temperature error, $\hat{Y}$, is

$$\hat{Y} = X\,b. \tag{10}$$

6. RESULTS

All eight target space parameters described previously were varied in this study. The physics model consists of the DIRSIG and MODTRAN tools. A UNIX script was written to easily change these parameter values in the DIRSIG and MODTRAN models. The values for each parameter are summarized in Table 1. The values for each parameter were chosen to cover the range of possible values for an actual dataset obtained at SRNL.

Int. Temp. [K]	**Ext. Temp. [K]**	**Fan** ε	**Sky Temp. [K]**	**Angle [°]**	**Amb. Temp. [K]**	**Amb. Dew Pt. [K]**	**Plume Length [m]**
290	Int. Temp. - 0	0.95	276.15	0	290	Amb. Temp. - 1	5
295	Int. Temp. - 2	0.80	262.40	10	294	Amb. Temp. - 5	10
300	Int. Temp. - 4	0.65	245.97	20	298	Amb. Temp. - 10	20
305			218.62	30			50
			203.09				100

Table 1. MDCT parameter values used for this LUT

The DIRSIG simulation was set at midnight local time. There was no atmospheric transmission loss or path radiance. Therefore, the DIRSIG simulation represents the tower-leaving radiance. Each run produced a spatially and spectrally over-sampled radiance image. The images were 110 by 110 pixels with a GSD of 0.05 meters. There were 746 spectral channels spanning approximately 1425 to 680 wavenumbers at a resolution of one wavenumber. This corresponds to roughly 7.0 to 14.7 μm in wavelength. The MODTRAN simulation, representing the plume, produced spectral transmission and path radiance curves for the same spectral range and resolution as the DIRSIG simulations. Midwave infrared wavelengths may be included in the target space if desired by running the DIRSIG and MODTRAN models for the appropriate wavelengths.

The DIRSIG and MODTRAN simulations were run on the research computing cluster at RIT. The machine consists of ninety-six 64-bit x86 processor cores running at approximately 3 Ghz. A single DIRSIG simulation runs in roughly 2.5 days on a single core. A single MODTRAN simulation runs in approximately one second on a single core.

For this study, the blurring effect of the sensor was chosen to be ignored. Therefore, only a spectral sampling was performed on the over-sampled radiance images. No spatial blurring was performed. The sensor spectral response was unity between 8.0 and 14.0 μm with a resolution of 0.3 μm.

The resulting temperature errors can be organized into a LUT that lists the temperature error for the mixed and cavity ROI for every combination of parameter values. The model predictors are the *MDCT external temperature*, the *fan blade emissivity*, the *sky temperature*, the *sensor zenith angle*, the *ambient air temperature*, the *ambient dew point temperature*, and the *plume path length* are labeled x_1 through x_7, respectively. The temperature error for the mixed ROI is labeled y_1 while the cavity ROI is labeled y_2. The parameter labels are included in Table 2 for reference.

Label	**Physical Term**
x_1	*MDCT External Temperature*
x_2	*Fan Blade Emissivity*
x_3	*Sky Temperature*
x_4	*Sensor Zenith Angle*
x_5	*Ambient Air Temperature*
x_6	*Ambient Dew Point Temperature*
x_7	*Plume Path Length*
y_1	*Temperature Error (Mixed ROI)*
y_2	*Temperature Error (Cavity ROI)*

Table 2. MDCT parameter values used for this LUT

Statistical analysis was performed on this 32,400 element dataset. The Minitab statistical software was used for the regression analysis. The resulting multiple linear regression equation for the mixed ROI temperature error is

$$\begin{aligned}\hat{y}_1 &= -17.2534 - 0.0340224\,x_1 + 11.2511\,x_2 + 0.0357615\,x_3 \\ &\quad - 0.0068026\,x_4 + 0.019290\,x_5 + 0.001709\,x_6 + 0.0023038\,x_7. \end{aligned} \tag{11}$$

This regression equation predicts the mixed ROI temperature error, $\hat{y}_1$, given the seven predictors, x_1 through x_7, described previously. This regression is valid for the range of parameters listed in Table 1.

To investigate the sensitivity of the regression equation, a regression analysis may be performed on standardized variables. Standardization involves transforming a variable so that it has a mean of zero and a standard deviation of one [12]. This is accomplished by subtracting the mean from every observation of a variable and then dividing by the standard deviation of the observations. The standardization makes it easier to compare the relative magnitudes of the different regression coefficients since the variables all have a variance of one.

The standardized regression equation for the mixed ROI case calculated in Minitab is

$$\begin{aligned}\hat{y}_{1s} &= 0.000000 - 0.106243\,x_{1s} + 0.738871\,x_{2s} + 0.518510\,x_{3s} \\ &\quad - 0.040781\,x_{4s} + 0.033781\,x_{5s} + 0.004510\,x_{6s} + 0.043430\,x_{7s}. \end{aligned} \tag{12}$$

The unstandardized regression coefficients measure the expected change in the response variable, $\hat{y}_1$, associated with a one unit change in the predictor variables. Therefore, the standardized regression coefficients measure the expected standard deviation change in the dependent variable associated with a one standard deviation change in the independent variable.

For the mixed ROI standardized regression equation, the fan emissivity parameter, x_2, has the highest standardized coefficient which signifies that the temperature error is most sensitive to the fan emissivity. This makes physical sense since for the mixed ROI, the fan emissivity variable affects both the self-emitted radiance of the pixel and also affects the reflected background radiance of the pixel.

The multiple linear regression equation for the cavity-only ROI temperature error calculated in Minitab is

$$\begin{aligned}\hat{y}_2 &= 0.67484 - 0.0193120\,x_1 - 0.000000\,x_2 + 0.00000000\,x_3 \\ &\quad - 0.00000000\,x_4 + 0.0189788\,x_5 - 0.0019372\,x_6 - 0.00196813\,x_7. \end{aligned} \tag{13}$$

This regression equation predicts the cavity ROI temperature error, $\hat{y}_2$, given the seven predictors, x_1 through x_7, described previously. The corresponding standardized regression equation for the cavity ROI case calculated in Minitab is

$$\begin{aligned}\hat{y}_{2s} &= 0.000000 - 0.611796\,x_{1s} + 0.000000\,x_{2s} + 0.000000\,x_{3s} \\ &\quad + 0.000000\,x_{4s} + 0.337175\,x_{5s} - 0.051861\,x_{6s} - 0.376387\,x_{7s}. \end{aligned} \tag{14}$$

For this case, the highest coefficient occurs for the *MDCT external temperature* parameter. Caution must be taken in interpreting this result. Recall that only a spectral integration was performed on the over-sampled images. There was no spatial blurring of the images for this study. Unlike for the mixed ROI case, the cavity ROI does not include any pixels from the fan. Therefore, the only influence on the temperature error for the cavity pixel should be due to the plume. The DIRSIG parameters should have coefficients of zero, as the fan blade emissivity, the sky temperature, and the sensor zenith angle do. It is unclear why the high coefficient of the *MDCT external temperature* parameter occurs. However, the non-zero coefficients on the MODTRAN parameters agree with the physical understanding that the plume should be the only influential parameter over the temperature errors in the cavity ROI case.

Finally, the 32,400 observations for each parameter were used as input into the unstandardized regression equations. The root-mean-square of the residuals was computed. For the mixed ROI regression equation, the RMS error was 0.767 K. The RMS error for the cavity ROI regression equation was 0.115 K. These RMS values represent an initial estimate of the error in the temperature correction factor.

7. SUMMARY

The exit air temperature of a mechanical draft cooling tower can be derived from a remotely-sensed thermal image. A physics model was used to simulate and predict the radiance reaching the sensor from the MDCT. The sensor-reaching radiance was then passed through a sensor model which converted the radiance into a digital image for that sensor. The apparent temperature of the MDCT is extracted from this simulated image. A target space is generated by running the physics and sensor models for a range of scene parameters. A temperature correction factor was defined as the difference between the apparent temperature and the assigned MDCT temperature in the physics model. A LUT was created that lists the temperature correction for each combination of model parameter values. This dataset was used to derive a parameterized function to predict the temperature correction necessary to derive the exit air temperature from a thermal image given some knowledge of the scene. The results indicate that the MDCT temperature error can be corrected to within 0.767 Kelvin and 0.115 Kelvin for the mixed ROI and cavity-only ROI cases, respectively.

ACKNOWLEDGMENTS

The authors would like to extend a special thanks to Paul Mezzanini of RIT Research Computing, to the DIRS laboratory at the Center for Imaging Science at RIT, and to the Savannah River National Laboratory for their sponsorship under contract DE-AC09-96SR18500.

REFERENCES

[1] Schott, J. R., [*Remote Sensing: The Image Chain Approach*], Oxford University Press, New York, NY (1997).

[2] Hecht, E., [*Optics*], Addison-Wesley Publishing Company, Reading, Massachusetts, second ed. (1990).

[3] Schott, J. R., Brown, S. D., Raqueño, R. V., Gross, H. N., and Robinson, G., "An advanced synthetic image generation model and its application to multi/hyperspectral algorithm development," in [*Canadian Journal of Remote Sensing*], **25**(2), 99–111 (1999).

[4] Berk, A., Bernstein, L. S., and Robertson, D. C., "MODTRAN: A moderate resolution model for LOWTRAN 7," Tech. Rep. GL-TR-89-0122, Spectral Sciences, Inc., Burlington, MA (April 1989).

[5] Montanaro, M., Salvaggio, C., Brown, S. D., Messinger, D. W., Goodenough, A. A., Garrett, A. J., and Villa-Aleman, E., "Radiometric modeling of cavernous targets to assist in the determination of absolute temperature for input to process models," in [*Proceedings of the SPIE, Sensor Data Exploitation and Target Recognition, Algorithms and Technologies for Multispectral, Hyperspectral, and Ultraspectral Imagery XIII*], 656511, Vol. 5806 (2007).

[6] Ward, G. J., "Measuring and Modeling Anisotropic Reflection," in [*Computer Graphics*], 265–272 (July 1992).

[7] "Nonconventional Exploitation Factors (NEF) Modeling," Tech. Rep. v9.5 (April 2005).

[8] Montanaro, M., Salvaggio, C., Brown, S. D., Messinger, D. W., and Garrett, A. J., "Apparent temperature dependence on localized atmospheric water vapor," in [*Proceedings of the SPIE, Sensor Data Exploitation and Target Recognition, Algorithms and Technologies for Multispectral, Hyperspectral, and Ultraspectral Imagery XIII*], 696618, Vol. 6966 (2008).

[9] Healey, G. and Slater, D., "Models and methods for automated material identification in hyperspectral imagery aquired under unknown illumination and atmospheric conditions," in [*IEEE Transactions on Geoscience and Remote Sensing*], **37**(6), 2706–2717, IEEE (1999).

[10] Ientilucci, E. J. and Schott, J. R., "Physics based target detection using a hybrid algorithm with an infeasibility metric," in [*IEEE International Conference on Acoustics, Speech, and Signal Processing (ICASSP)*], 1193–1196, IEEE ICASSP Vol. 5, Toulouse, France (May 2006).

[11] Neter, J. and Wasserman, W., [*Applied Linear Statistical Models: regression, analysis of variance, and experimental designs*], Richard D. Irwin, Inc., Homewood, Illinois (1974).

[12] L.Mason, R., Gunst, R. F., and Hess, J. L., [*Statistical Design and Analysis of Experiments with applications to engineering and science*], John Wiley & Sons, Inc., New York, NY (1989).